Available online at www.sciencedirect.com
ScienceDirect
Acta Materialia 58 (2010) 5481–5490
Acta MATERIALIA
www.elsevier.com/locate/actamat

Interactions between carbon solutes and dislocations in bcc iron

Y. Hanlumyuang [a,*], P.A. Gordon [b], T. Neeraj [b], D.C. Chrzan [a]

[a] Materials Science and Engineering, University of California, Berkeley, CA 94720, USA
[b] Corporate Strategic Research, ExxonMobil Research and Engineering, Annandale, NJ 08801, USA

Received 12 February 2010; received in revised form 26 May 2010; accepted 12 June 2010
Available online 9 July 2010

Abstract

Carbon solute–dislocation interactions and solute atmospheres for both edge and screw dislocations in body-centered cubic (bcc) iron are computed from first principles using two approaches. First, the distortion tensor and elastic constants entering Eshelby's model for the segregation of C atoms to a dislocation core in Fe are computed directly using an electronic-structure-based the total energy method. Second, the segregation energy is computed directly via first-principles methods. Comparison of the two methods suggests that the effects of chemistry and magnetism beyond those already reflected in the elastic constants do not make a major contribution to the segregation energy. The resulting predicted solute atmospheres are in good agreement with atom probe measurements.

Keywords: Ferritic steels; Dislocations; Solute segregation; Total energy calculations

1. Introduction

The mechanical properties of ferritic Fe–C alloys such as yield points, ductilities and toughnesses are influenced by the solute atmosphere around dislocations [1]. In addition to lattice friction, solutes may exert pinning forces that further impede dislocation plasticity. Sharp yield points or strain aging results from a static atmosphere at low temperature, while a mobile atmosphere at intermediate temperature results in dynamics strain aging or the Portevin–Le Chatelier effect [2]. Designing new ferritic alloys or other materials depends on the accuracy of probing and predicting the properties of the solute atmosphere.

Imaging the solute atmosphere of C atoms in ferritic Fe–C alloys has been made possible only recently using atom probe tomography [3]. The extent of spreading of the solute atmosphere is of the order of 10 nm, while the enrichment factor, the ratio of the concentration of solute in the neighborhood of the dislocation over the matrix concentration, is approximately 7.7 (within the considered region). Both the extent of spreading and concentration of solute atoms implies that much of the atmosphere resides far from the elastic singularity of the core (the region within approximately one Burgers vector of the core, where bonding topology differs substantially from the bulk crystalline counterparts). In regions remote from the core, elasticity theory should be suitable for predicting defect interactions and carbon solute atmospheres.

The elasticity theory of carbon solute–dislocation interactions has been extensively studied. Cochardt et al. [4] studied the interaction using isotropic linear continuum elasticity theory to describe the dislocations. A similar theory was formulated by Bacon [5], where the tetragonal distortion of the interstitial solute was modeled as an elastic dipole tensor. Anisotropic linear continuum elasticity theory was later employed in the work by Douthwaite and Evans [6]. The most recent published work represents a conjunction of elasticity theory and atomic scale simulations [7].

The maximum solute–dislocation interaction energies from these models are summarized in Table 1. Note that the predicted maximum of the solute interaction energy with screw dislocations based on elasticity theory is about 75% of that for edge dislocations. Also, the variation of

* Corresponding author. Tel.: +1 510 642 8484; fax: +1 510 643 5792.
E-mail address: yhanlumy@berkeley.edu (Y. Hanlumyuang).

1359-6454/$36.00 © 2010 Acta Materialia Inc. Published by Elsevier Ltd. All rights reserved.
doi:10.1016/j.actamat.2010.06.024

Table 1
Elasticity theory predictions of solute–dislocation interaction energies. The maximum interaction energy is calculated at $r = |\mathbf{b}|$.

References	Dislocation type	Dislocation models	Distortion type	Maximum interaction energy (eV)
[1]	Edge	Isotropic	Isotropic	–
[4]	Edge, screw	Isotropic	Tetragonal	0.75, 0.75
[5]	Edge, screw	Isotropic	Tetragonal	0.49, 0.37
[6]	Screw	Anisotropic	Tetragonal	0.60
[7]	Edge, screw	Anisotropic	Tetragonal	0.40, 0.30

the maximum interaction energies within these studies varies by more than a factor of 2. Clearly, further detailed theoretical studies of solute–dislocation interaction and solute atmospheres are still needed.

Differences in the maximum interaction energies reported in Table 1 stem from two sources: variations in (1) the assumed elastic constants, and (2) the amount of distortion induced by a carbon interstitial.

Experimentally, there have been attempts to measure the lattice distortion induced by a single solute atom. Typically, the lattice parameter of Fe–C martensite is used to measure the strain. A large variation of data on lattice parameter changes with carbon content has been observed [11]. The scatter arises from experimental errors due to different methods employed for lattice parameter determination and the existence of residual stresses from quenching the austenite that might suppress lattice parameter changes. Another possible source of error is the effect of equivalent interstitial sites. Since carbon atoms can fill one of the three equivalent octahedral sites in body-centered cubic (bcc) iron, the resultant average deformation may trend toward isotropic, rather than tetragonal. Despite these issues, experimental results appear to have converged. Fig. 1 replots the data from Refs. [8–10] as considered and plotted in Ref. [11]. The experiments indicate that the lattice parameters of Fe–C alloys depend linearly on C composition for the studied range.

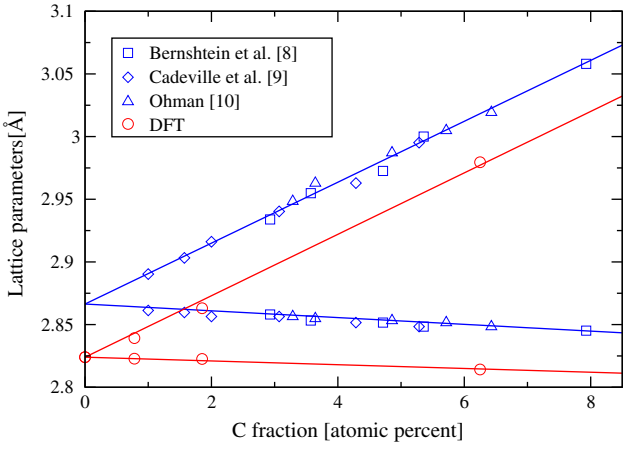

Fig. 1. Least-square fits of lattice parameters (a, c) computed from first-principles as functions of the number of C atoms. The least-square fits of experimental data originally reported in Refs. [8–10], and collected by Cheng et al. [11] are also plotted. The calculated and experimental data are not scaled to the same origin.

Theoretically, the most fundamental study of defect interactions is due to Eshelby [12,13]. Eshelby has shown that the tetragonal solute–dislocation interaction energy is the product of the strength of the point source and the strain field produced at the point source by the dislocation. In this work, we revisit this model and show that Eshelby's formulation can be complemented by first-principles calculations based on density functional theory (DFT) [14]. Specifically, the strength of the point source and the elastic constants entering Eshelby's expressions can be computed directly using electronic-structure-based total energy methods. Further, electronic structure methods can be used to compute the segregation energy directly. This more direct approach yields the correct continuum limit and can, potentially, reveal chemical and magnetic contributions to the interaction beyond those already reflected within the elastic constants and distortion tensor. Further, the direct approach may be extended to high-strain situations, where linear elasticity theory may no longer be valid.

The theoretical basis of the calculations is developed in Section 2. The ab initio calculations and results for a dilute Fe–C alloy are described in Section 3. In Section 4, the theory is used to compute the distribution of C solute atoms around edge and screw dislocations in Fe.

2. Computational approach

Eshelby has shown that by regarding the solute atom as a point source of stress, particularly for one where the forces are unequal along the horizontal and vertical axes [12], the interaction energy of the solute and the dislocation is:

$$F^{int} = -\Gamma^o_{ij}\Delta^d_{ij}, \tag{1}$$

where Γ^o_{ij} is the strength of the point source, and Δ^d_{ij} is the distortional field produced at the source by the dislocation. The strength of the source Γ^o_{ij} is the elastic dipole moment of the solute atom [15,16]. It is a function of the electronic structure differences and bonding between the host atoms and the solute atom.

In principle, computing Γ^o_{ij} using atomic scale approaches should be straightforward. One simply includes an interstitial atom within an Fe crystal, and measures the displacements of the atoms within the crystal. In practice, however, the procedure is more complex. The best electronic-structure-based total energy methods are computationally expensive and work best for periodic systems.

Hence the computation of segregation energy is most conveniently carried out using supercells and periodic boundary conditions. The relationship between periodic supercells and the desired quantities, however, can be obtained readily. In the Appendix it is shown how the strength of the point source can be computed using a periodic supercell approach, and this is the approach applied to the present case.

Within the bcc structure there are three types of octahedral interstitials, indicated by the axis along which the primary axis of the octahedron lies. The respective Γ^o's are defined to be

$$\mathbf{\Gamma}^{o(1)} = \begin{pmatrix} \Gamma^o_{11} & 0 & 0 \\ 0 & \Gamma^o_{22} & 0 \\ 0 & 0 & \Gamma^o_{22} \end{pmatrix}, \quad \mathbf{\Gamma}^{o(2)} = \begin{pmatrix} \Gamma^o_{22} & 0 & 0 \\ 0 & \Gamma^o_{11} & 0 \\ 0 & 0 & \Gamma^o_{22} \end{pmatrix}$$
$$\mathbf{\Gamma}^{o(3)} = \begin{pmatrix} \Gamma^o_{22} & 0 & 0 \\ 0 & \Gamma^o_{22} & 0 \\ 0 & 0 & \Gamma^o_{11} \end{pmatrix}, \tag{2}$$

where the superscripts (i) indicate the dipole strength for an interstitial in the octahedral site with primary axis (i.e. the 4-fold axis) along the ith direction.

As shown in Appendix A, the elastic dipole moment is related to the change in lattice parameters upon relaxing a periodic structure with one C atom per Fe supercell. For a carbon solute located along the x_1-axis of a simulation block defined by parameters L_1, L_2 and L_3, the components of the elastic dipole moment are (Eq. (A22)):

$$\begin{aligned} \Gamma^o_{11} &= v_o(C_{11}\eta^c + 2C_{12}\eta^a), \quad \text{and} \\ \Gamma^o_{22} &= v_o(C_{11}\eta^c + C_{12}(\eta^c + \eta^a)), \end{aligned} \tag{3}$$

where v_o is the primitive cell volume, and C_{11} and C_{12} are two of the cubic elastic constants. The parameters η^c and η^a measure the relative changes in the supercell lattice parameters with respect to an addition of a C solute atom:

$$\eta^c = \frac{1}{L_o}\frac{dL_1}{dn}\bigg|_{n=0}, \quad \text{and} \quad \eta^a = \frac{1}{L_o}\frac{dL_2}{dn}\bigg|_{n=0}, \tag{4}$$

where η^c measures the expansion of the unit cell along the primary axis of the occupied octahedron, and η^a measures the contraction along the perpendicular axes. Here, n is the interstitial mole fraction of the C solute or the ratio between the number of C atoms to the host Fe atoms. η^a and η^c are determined by considering the relaxation of supercells of varying compositions and plotting the observed lattice parameters as a function of n. These calculations are presented in Section 3.

In an alternative approach, the energy in Eq. (1) can be computed without the need to determine explicitly the η's. The solute atom–dislocation interaction can be computed directly using periodic supercell calculations. Each supercell contains one solute atom, and the dislocation is assumed to strain the supercell homogeneously and externally to the cell [17–20]. The addition of the strain and stress fields of dislocation induces a variation in the strain energy. This variation defines the interaction energy between solute and dislocation.

The action of the dislocation on the solute is enforced using a fixed strain boundary condition. This choice is illustrated in Fig. 2 along with a stress-controlled alternative. It is more convenient to perform atomic simulation using strain-controlled boundary conditions. In the case of strain-controlled boundary conditions, the boundary of the simulation supercell is fixed after applying a constant traction T^d_{ij} due to the dislocation stress field. The supercell (and its periodic images) is then held at a constant external dislocation strain field ε^d_{ij} (Fig. 2A). The supercell is brought in contact only with a thermal reservior while remaining mechanically isolated. The governing thermodynamics potential is thus the Helmholtz free energy F.

To extract the interaction energy that, in the continuum limit, reduces to Eshelby's result in Eq. (1), the interaction is defined as the difference between the segregation energy of the solute in a strained vs. an unstrained state, i.e.

$$F^{int} = [F(Fe:C, \boldsymbol{\varepsilon}^d) - F(Fe, \boldsymbol{\varepsilon}^d)] - [F(Fe:C) - F(Fe, ref)], \tag{5}$$

where $F(Fe:C, \boldsymbol{\varepsilon}^d)$ is the energy of cells containing mostly Fe atoms and a C atom with an imposed uniform dislocation strain $\boldsymbol{\varepsilon}^d$. $F(Fe, \boldsymbol{\varepsilon}^d)$ is the energy of cells containing only Fe under the strain $\boldsymbol{\varepsilon}^d$. $F(Fe:C)$ is the energy of the octahedral defect and $F(Fe, ref)$ is the energy of the reference perfect lattice.

Eq. (1) is the continuum linear elastic limit of Eq. (5). A new variable $\bar{\Delta}^c_{ij} = \partial_j \bar{u}^c_i$ is defined as the distortional field of the solute under the strain-controlled boundary conditions. The fixed strain boundary conditions imply that:

$$\int_\Omega \bar{\Delta}^c_{ij} dV = 0, \tag{6}$$

where the integral extends over the supercell volume, Ω.

The external dislocation field Δ^d_{ij} simply adds to the solute fields $\bar{\Delta}^c_{ij}$, and the relaxation energy from Eq. (A3) becomes:

$$\begin{aligned} \Delta F' &= F(Fe:C, \boldsymbol{\varepsilon}^d) - F(Fe, ref) \\ &= \int_\Omega \left[\sigma^o_{ij}\left(\bar{\Delta}^c_{ij} + \Delta^d_{ij}\right) + \frac{1}{2} c_{ijkl}\left(\bar{\Delta}^c_{ij} + \Delta^d_{ij}\right)\left(\bar{\Delta}^c_{kl} + \Delta^d_{kl}\right) \right] dV. \end{aligned} \tag{7}$$

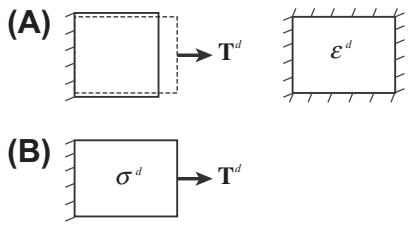

Fig. 2. Schematic illustrations of two types of boundary conditions. (A) Strain-controlled: changes in shape and volume of the body are produced by the traction $\mathbf{T}^d$, and once the traction is removed, the body is fixed by a constant strain $\boldsymbol{\varepsilon}^d$. (B) Stress-controlled: a constant traction $\mathbf{T}^d$ is held constant while the boundary is not fixed. The figures are drawn after Refs. [19,20].

Applying Eqs. (A9) and (6), the relaxation energy can be written as:

$$\Delta F' = \int_\Omega \left(\sigma^o_{ij} \bar{\Delta}^c_{ij} + \frac{1}{2} c_{ijkl} \bar{\Delta}^c_{ij} \bar{\Delta}^c_{kl} \right) dV + \frac{1}{2} \Omega c_{ijkl} \Delta^d_{ij} \Delta^d_{kl} - \Gamma^o_{ij} \Delta^d_{ij}. \tag{8}$$

Here, σ^o_{ij} is the strain-free stress required to maintain the reference structure upon an insertion of the carbon solute.

The free energy of the system with constant external applied strain is:

$$\Delta F^d = F(Fe, \varepsilon^d) - F(Fe, ref) = \frac{1}{2} \Omega c_{ijkl} \Delta^d_{kl} \Delta^d_{ij}. \tag{9}$$

The free energy of the solute in the absence of the dislocation traction field is:

$$\begin{aligned} \Delta F^c &= F(Fe:C) - F(Fe, ref) \\ &= \int_\Omega \left(\sigma^o_{ij} \bar{\Delta}^c_{ij} + \frac{1}{2} c_{ijkl} \bar{\Delta}^c_{ij} \bar{\Delta}^c_{kl} \right) dV. \end{aligned} \tag{10}$$

The interaction free energy approximated by linear elasticity theory is then given by:

$$F^{int} = \Delta F' - \Delta F^d - \Delta F^c = -\Gamma^o_{ij} \Delta^d_{ij}, \tag{11}$$

which is in agreement with Eq. (1). Thus, within the strain-controlled boundary condition, the ab initio calculations are simple and also yield a continuum limit in agreement with Eshelby's result. Moreover, since the strain field can be chosen beyond those described by linear elasticity theory, Eq. (5) is a generic expression for the interaction of a defect with an arbitrary amplitude applied field (admittedly within a uniform strain approximation). Further, contributions of magnetism and higher-order elastic moduli to interactions, commonly ignored in the elasticity theory, are intrinsically included in Eq. (5). Comparisons of the results derived from Eq. (5) with those derived from Eq. (1) enable assessment of the influence of magnetic and electronic effects beyond those already reflected in the elastic constants [21].

As a final step in the analysis, the solute atmosphere of a dislocation is determined using the computed energies and a simple statistical mechanics model. The predicted solute atmospheres around edge and screw dislocations along with experimental comparison are presented in Section 4.

3. Solute–dislocation interactions

In this section, first-principles electronic-structure-based total energy methods are applied to calculate the solute atom–dislocation interaction energy. These calculations make use of the approaches described above (and in the appendix), and the predictions from both methods are compared. It is important to note that these electronic structure calculations do not include an explicit dislocation core. Consequently, total energy calculations based on empirical interatomic potentials are used to assess the range of validity for the methods.

Electronic-structure-based total energy calculations are performed using the Vienna Ab initio Simulation Package (VASP) [22]. The pseudopotentials describing the electron–ion interaction are generated by the projector augmented wave (PAW) method within the spin-polarized generalized gradient approximation (GGA).

Elastic moduli and bulk structural properties are computed using a plane-wave expansion with an energy cutoff of 370 eV. A $17 \times 17 \times 17$ symmetrized Monkhorst–Pack grid is used for all integrations. This energy cutoff and grid sufficiently converge the total energy to better than 0.06 meV/atom. The values reported by Clatterbuck et al. [23], the present results and experimental results [11,24] are summarized in Table 2. The present results agree well with prior calculations.

Previous theoretical determinations of the solute–dislocation interaction energy have been done using experimental values of the lattice parameter changes in Fe–C martensitic transformations [4–6]. The lattice parameters reported in these efforts were obtained from X-ray measurements of the mean tetragonal distortion of martensite. Clouet et al. [7], on the other hand, computed the interaction energy using the lattice parameters from atomic simulation based on empirical potentials. Here, the relative lattice contraction and expansion, η^a and η^c, are computed by relaxing supercells containing host Fe atoms and a C interstitial atom with respect to changes in volume and internal coordinates. The calculations are performed with supercells containing 16, 54 and 128 Fe atoms. To converge the total energy of the Fe–C alloy structures, the energy cutoff for all cells is set to 400 eV. (This cutoff is greater than the 370 eV used in determining the elastic constants mainly because of the C atom in the structure.) The k-point grids are adjusted so that the reciprocal volume per k-point for different sized supercells remains approximately unchanged. Specifically, a grid of $6 \times 6 \times 6$, $4 \times 4 \times 4$ and $3 \times 3 \times 3$ is used for the 16, 54 and 128 Fe atom supercells, respectively. This number of k-points and the energy cutoff sufficiently converge the total energy of the relaxed Fe–C alloy structure better than 0.06 meV/atom, and forces on the atoms are converged to less than 0.001 eV/Å. The concentration dependence of the lattice parameter predictions is also shown shown in Fig. 1. Note that the predicted equilibrium lattice parameter for Fe is less than that measured experimentally. The dependence of the lattice parameter on composition, however, tracks the experimental data compiled by Cheng et al. [11]. The resulting values of η_c and η_a are shown in Table 2. The computed values for η_c, η_a and the elastic moduli are then incorporated into Eqs. (1) and (3) to compute the C solute atom–dislocation interaction.

In evaluating the atomistic interaction energy of a C solute atom with an edge dislocation of type $\langle 1\,1\,1 \rangle \{0\,1\,1\}$ based on Eq. (5), the local change in concentration $\Delta n^{(m)}$ is fixed by the size of the supercell. In the present study, the supercells of 54 Fe atoms and one C interstitial are employed, hence the local composition is $n^{(m)} = 1/54$. Total

Table 2
Bulk properties of pure iron and the relative lattice expansion and contraction due to a C atom located at an octahedral interstitial site.

	PAW (this work)	EAM (this work)	PAW [23]	Exp. [11,24]
a_o (Å)	2.824	2.856	2.830	2.86
C_{11} (GPa)	282	244	286	245
C_{12} (GPa)	153	144	147	139
C_{44} (GPa)	99	116	99	122
η^a	−0.053	−0.087		−0.094
η^c	0.867	0.550		0.847

energy calculations are performed using k-point $5 \times 5 \times 5$ Monkhorst–Pack k-point mesh and a 400 eV energy cutoff. For the Fe–C alloy structure in the strain-controlled boundary conditions, this k-point mesh and energy cutoff converge the total energy to better than 0.06 meV/atom. The cell volumes and lattice vectors used in the calculation are fixed by the anisotropic dislocation strain [2,25]. Internal atomic positions are fully relaxed.

Fig. 3 shows the angular dependence of the solute–dislocation interaction energies computed using Eq. (5) together with predictions from periodic elasticity theory, Eq. (1). The energies are evaluated at a radial distance of 12 Å from the dislocation core. A general trend of solute attraction (repulsion) below (above) the dislocation slip plane is observed. Both the tetragonality of the solute and the anisotropicity of the elastic fields give rise to the angular dependence of the amplitude of the interaction. Excellent agreement between atomistic and periodic elasticity theory predictions confirms (in part) the applicability of the periodic elasticity theory at distances of 12 Å from the core and greater.

A remaining issue is to evaluate the minimum extent to which first-principles calculations and the periodic elasticity theory are valid in the core region. This is a non-trivial question. The dislocation core represents extremes in both stresses and stress gradients, as well as altered bonding topology. Since the periodic elasticity approach necessarily excludes stress gradients and altered bonding topologies, the theory is unlikely to be applicable at the core itself. Further, numerical limitations only enable the study of relatively small supercells using electronic-structure-based total energy methods. Consequently, it is difficult to study the interaction of a single solute atom with an extended dislocation using these methods. An alternative approach is to use empirical interatomic potential-based methods to assess the extent to which defect separations are amenable to linear elasticity theory.

The extent of defect separations at which the elasticity is valid is examined by similar calculations employing embedded atom method (EAM) [26,27] empirical potentials. Bulk properties obtained from this EAM empirical potential are summarized in Table 2. Similar studies of solute–dislocation interactions based on empirical potentials have been carried by several authors [7,28–31].

In computing an interaction energy using EAM empirical potentials, four independent calculations are necessary.

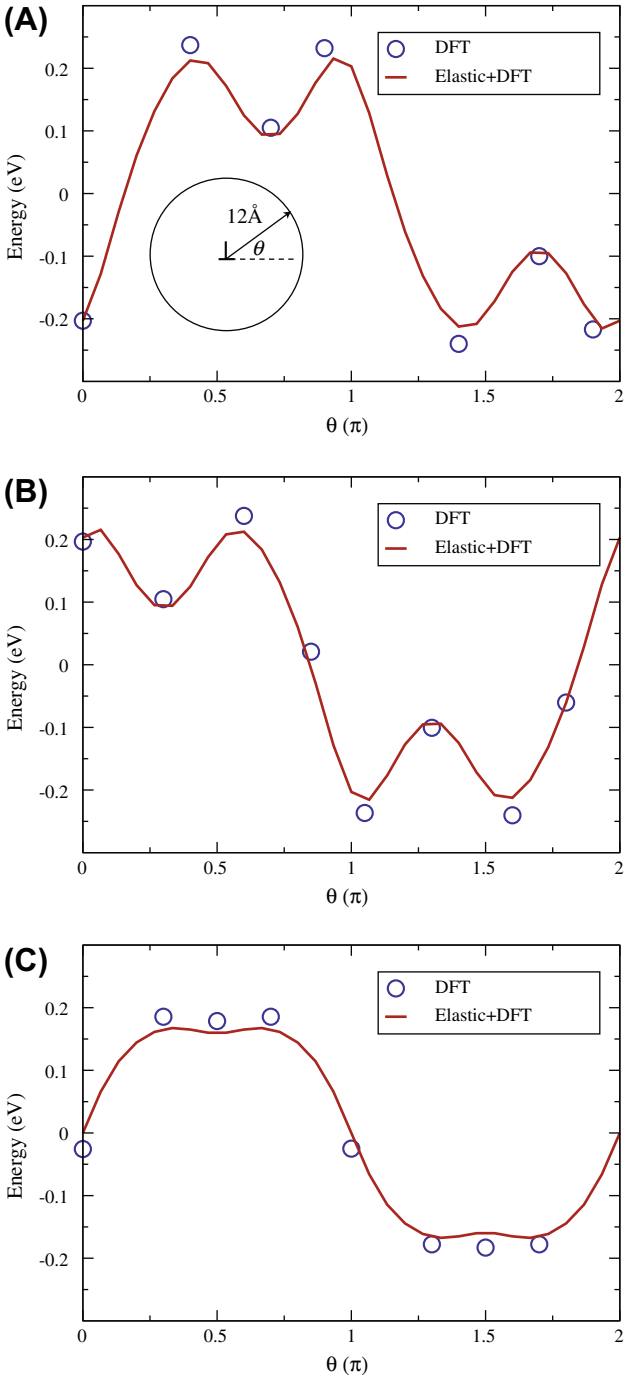

Fig. 3. Continuum and DFT-based interaction energy between a C solute atom and a $[111](1\bar{1}0)$ dislocation in Fe at 12 Å. The solute atom is located on x_1, x_2, and x_3-type sites in (A), (B) and (C), respectively.

The interaction energies extracted are similar to ones comprising Eq. (5), where $F(Fe:C,\boldsymbol{\varepsilon}^d)$ and $F(Fe,\boldsymbol{\varepsilon}^d)$ are replaced by energies of nonuniform strained cells. The calculation cell is oriented such that its x_1-axis is parallel to [1 1 1] and the x_2-axis to $[1\bar{1}0]$. Periodic boundary conditions are applied along the dislocation line, and the dislocation is placed on the neutral bending axis. Stationary boundary conditions are imposed in the x_1- and x_2-direction. Image effects are minimized by employing large calculation cells containing approximately 40,000 atoms with a dimension of 150 × 150 × 20 Å, as illustrated in Fig. 4.

Fig. 5 shows interactions between a ⟨1 1 1⟩{1 1 0} edge dislocation and a C solute atom computed from atomic simulations using the Fe–C empirical potential developed by Becquart et al. [32]. The energies are plotted at constant θ while varying the distance from the dislocation core. The angle θ is measured from the ⟨1 1 1⟩ axis. Solid lines are the interaction energies predicted from periodic elasticity theory. Except for the case $\theta = 0$, the energy interactions show continuous deviations from the elasticity theory at about three Burgers vectors from the dislocation core. In the case $\theta = 0$, the discontinuous variation of the energy is caused by the dislocation core shifting toward the solute. The high-strain region around the solute in this case enables total energy reduction by inducing motion of dislocation. However, no similar results are observed at the other angles. The minimum defect separation used in both the homogeneous strain approximation and the periodic elasticity theory is approximately 3*b*.

Since stress and strain field gradients are incorporated into the explicit solute–dislocation atomistic simulation, comparison between interactions computed from atomic simulations and the periodic elasticity theory enable an assessment of the importance of these gradients. As is shown in Fig. 6, the agreement between elasticity theory and the direct atomistic results is excellent beyond 3*b*. The agreement demonstrates the unimportance of strain gradients to solute atom–dislocation interactions, at least in the far-field as represented by EAM.

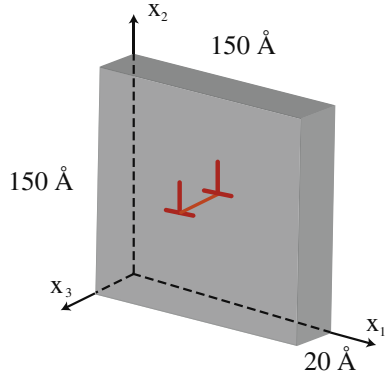

Fig. 4. A simulation cell for EAM calculations. The size of the cell is 150 × 150 × 20 Å, containing approximately 40,000 Fe atoms. The center of the cell contains an edge dislocation threading the bending axis.

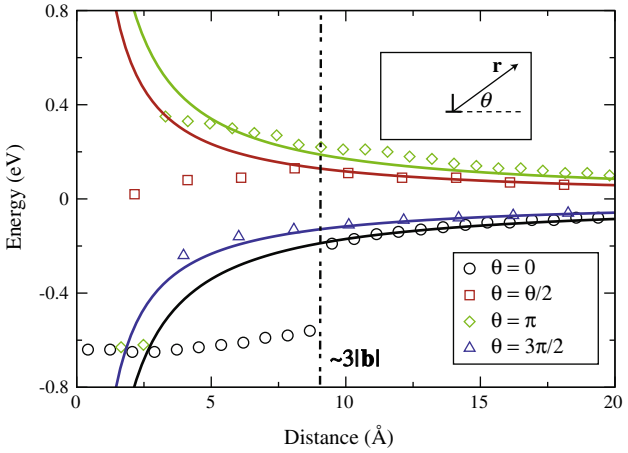

Fig. 5. Interaction energies between a C solute atom and a ⟨1 1 1⟩{1 1 0} edge dislocation in Fe computed from atomic simulation based on empirical potentials. The energies are measured as a function of distance from the dislocation core as depicted in the inset.

4. Solute atmosphere

Solutes and dislocation mapping within atom probe tomography provides perhaps the most direct information regarding solute atom–dislocation interactions [3]. First-principles calculations aid tomographic experiments by providing theoretical prediction of solute atmospheres.

As found by experiments [3], much of the solute atmosphere is distributed far from the dislocation core. In this far-field, the assumptions entering the periodic elasticity theory developed above should be acceptable.

Theoretical studies of solute atom distributions are rooted in a statistical mechanics model already pursued by several authors [33,34]. Since the occupancy state of the interstitial site by a solute atom is either zero or unity, Fermi–Dirac statistics are suitable for quantifying solute concentrations. Assuming solutes are non-interacting particles, the thermal average value of the occupancy of the interstitial sites is given by:

$$n^{(m)}(\mathbf{r}) = \frac{\exp\left[-\frac{\mu+F_{int}^{(m)}(\mathbf{r})}{kT}\right]}{1+\exp\left[-\frac{\mu+F_{int}^{(m)}(\mathbf{r})}{kT}\right]}, \tag{12}$$

where μ is the chemical potential of the solute. Away from the dislocation where the interaction energy is negligible, the occupancy of the interstitial sites is:

$$n_o^{(m)} = \frac{\exp\left[-\frac{\mu}{kT}\right]}{1+\exp\left[-\frac{\mu}{kT}\right]}. \tag{13}$$

By eliminating μ in Eqs. (12) and (13), the fraction of occupied interstices is given by:

$$\frac{n^{(m)}(\mathbf{r})}{1-n^{(m)}(\mathbf{r})} = \frac{n_o^{(m)}}{1-n_o^{(m)}}\exp\left[-\frac{F_{int}^{(m)}(\mathbf{r})}{kT}\right], \tag{14}$$

where the elastic interaction energy term is computed from Eq. (1).

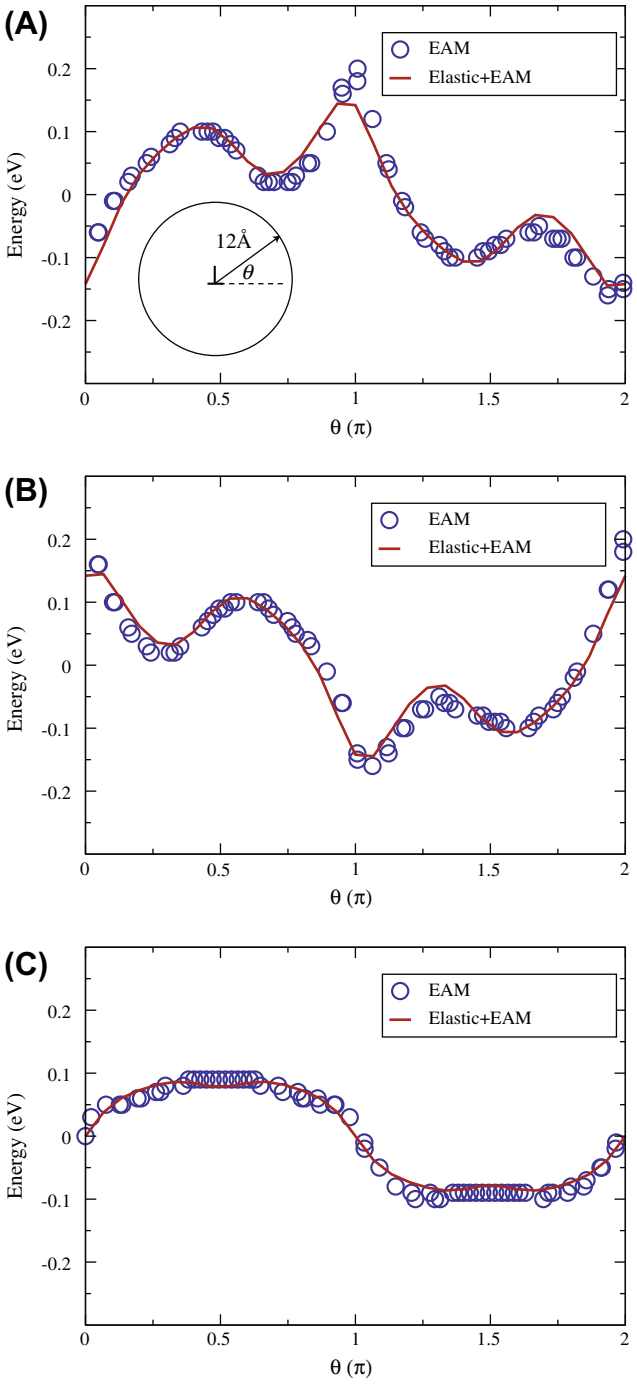

Fig. 6. Continuum and EAM-based interaction energy between a C solute atom and a $[111](1\bar{1}0)$ dislocation in Fe at 12 Å. The solute atom is located on the x_1, x_2, and x_3-type sites in (A), (B) and (C), respectively.

The net accumulation of solute is:

$$\Delta n = (n^{(1)} + n^{(2)} + n^{(3)}) - n_o \tag{15}$$

where in this work the background concentration n_o is assumed to be Fe–0.11 wt.% C or 0.5 at.% C as in the experiment in Ref. [3].

The first-principles predictions of solute atmospheres Δn as in Eq. (15) are shown in Figs. 7 and 8. The edge dislocation in Fig. 7 is of type $\frac{1}{2}[111](1\bar{1}0)$. There is a net accumulation of solute in the tensile region under the dislocation. The size of the solute cluster also depends on the temperature. A denser cluster of solutes is observed at the temperature 300 K. Fig. 8 shows a net concentration profile around a $\frac{1}{2}[111](11\bar{2})$ screw dislocation at room temperature. Since screw dislocations exert shear forces in the crystal, the change in solute concentration around them is less than that around edge dislocations. A 3-fold symmetry of solute distribution around the screw dislocation arises from a 3-fold crystal symmetry along [1 1 1] direction of a cubic crystal and the tetragonality of the solutes.

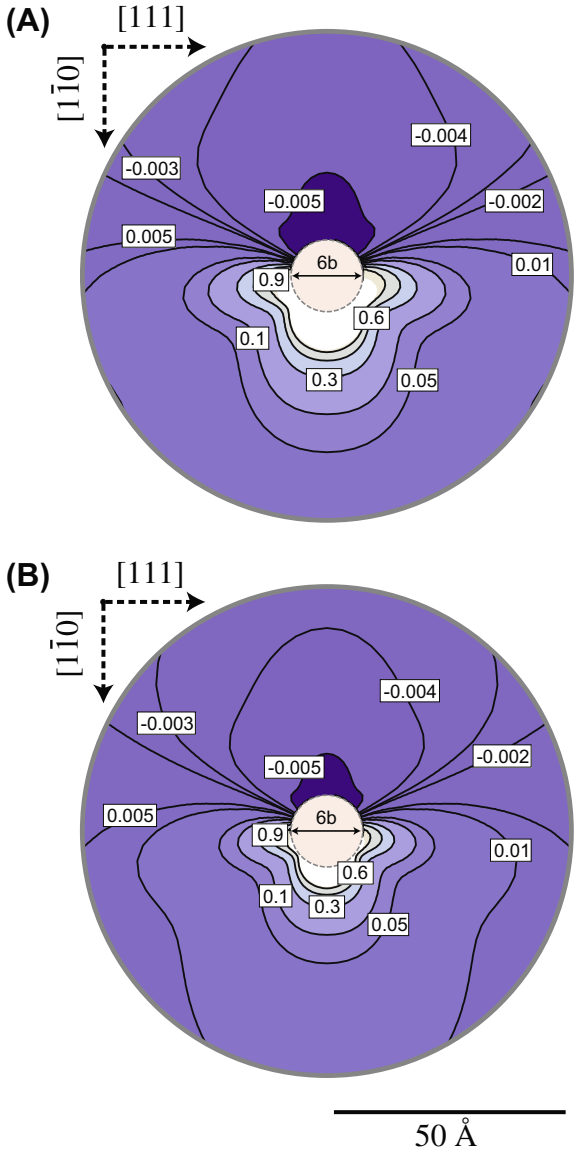

Fig. 7. Solute distributions around a $[111](1\bar{1}0)$ edge dislocation at temperatures of: (A) 300 K and (B) 400 K.

To a good approximation, C atoms are bound to the dislocation only when their interaction energy is larger than k_BT. Thermal fluctuation may take away C atoms at a distance when the interaction is small compared to the thermal energy. Setting the interaction energy equal to k_BT defines a region over which solute concentration

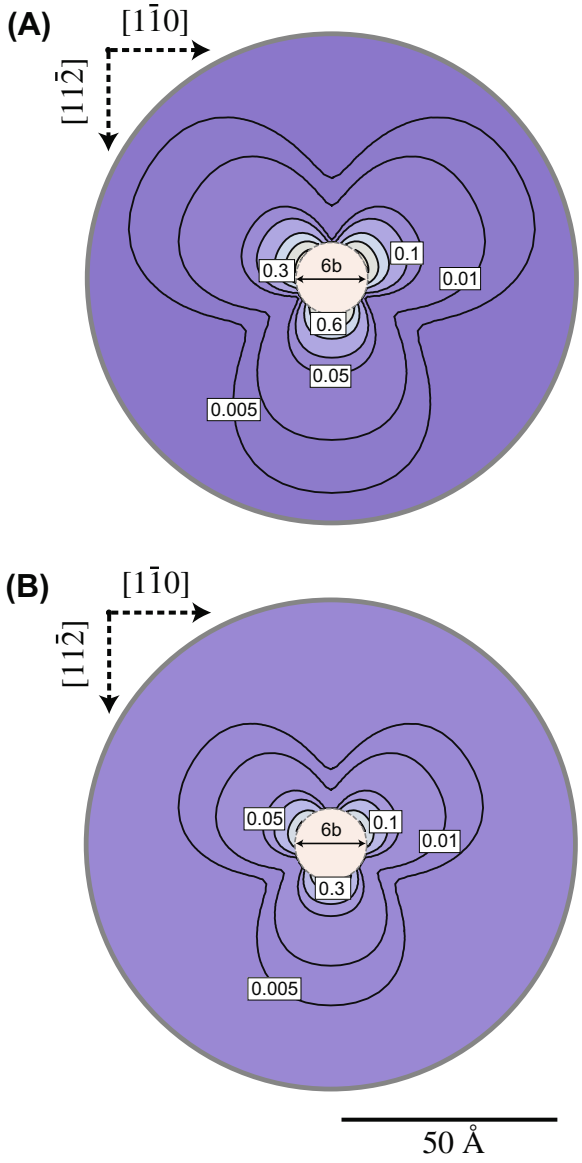

Fig. 8. Solute distributions around a [111](11$\bar{2}$) screw dislocation at temperatures of: (A) 300 K and (B) 400 K.

may be enhanced, and enables the definition of an enrichment factor. Table 3 reports this size for both edge and screw dislocations at 300 K. Quantitatively, the theoretical solute atmosphere spreads about 100–200 Å from the dislocation core in agreement reported values (~100Å) from atom probe experiments [3].

In the atom probe literature, the ratio of the number of the solute atoms to those of the background atoms is known as the enrichment factor. The predicted and experimental enrichment factors for 300 K are shown in Table 3. The theoretical value of the enrichment is most likely underestimated because the core region 6*b* in diameter is excluded in the calculation. If the solute segregation energies predicted by the theory are used to predict the carbon concentration within the core region, the predicted enrichment factors for both screw and edge dislocation rise to approximately 6.7. The resulting predictions of the theory are in reasonable agreement with experimental observations.

Table 3
Extent and enrichment of solute atoms around dislocations. The diameter 6*b* around the dislocation core is excluded in the prediction.

References	Dislocation type	Extent (nm)	Enrichment factor
This work	Screw	12	4.4
This work	Edge	20	5.3
[3]	Unknown	10	7.7

5. Summary

The C solute atmospheres near edge and screw dislocations in Fe are computed. The calculations are performed employing first-principles electronic structure total energy methods and periodic supercells, and, in the continuum limit, reduce to Eshelby's model for defect interactions. The resulting theory is expected to model accurately solute atom–dislocation interactions at distances greater than 3*b* from the origin of the dislocation. The predictions of the theory are in good agreement with experimental observations of solute atmospheres.

Acknowledgment

The authors gratefully acknowledge the support of ExxonMobil.

Appendix A. Periodic elasticity theory

Consider a solid modeled using a supercell. Each supercell has volume Ω. If a stress-free boundary condition is imposed, and in the limit of large Ω, insertion of a solute atom into an interstitial site within the supercell approximates a dilute Fe–C alloy. Insertion of the solute atom while not allowing relaxation leads to an elastic strain. The subsequent structural relaxation reduces the elastic energy. The relaxed energy per unit volume, $\Delta\phi$, can be approximated as a Taylor series in the solute distortion $\Delta^c_{ij}(\mathbf{r}) = \partial_j u^c_i(\mathbf{r})$ as [17,35,36]:

$$\Delta\phi = \left(\frac{\partial\phi}{\partial\Delta^c_{ij}}\right)_o \Delta^c_{ij} + \frac{1}{2}\left(\frac{\partial\phi}{\partial\Delta^c_{ij}\partial\Delta^c_{kl}}\right)_o \Delta^c_{ij}\Delta^c_{kl}, \tag{A1}$$

where the subscript *o* indicates the derivative at zero distortion, and the Einstein summation convention is employed.

By definition,

$$\sigma^o_{ij} = \left(\frac{\partial\phi}{\partial\Delta^c_{ij}}\right)_o, \quad \text{and} \quad c_{ijkl} = \left(\frac{\partial\phi}{\partial\Delta^c_{ij}\partial\Delta^c_{kl}}\right)_o, \tag{A2}$$

where σ^o_{ij} is the strain-free stress required to restore the perfect crystal reference state and the c_{ijkl} are the elastic constants. The first term in the right-hand side of Eq. (A1) is the energy required to take a single solute from a standard state and insert it into Ω without displacement of the host atoms.

The net relaxation energy due to the presence of a solute is:

$$\Delta F = \int_\Omega \Delta\phi dV = \int_\Omega \left(\sigma^o_{ij}\Delta^c_{ij} + \frac{1}{2}c_{ijkl}\Delta^c_{ij}\Delta^c_{kl}\right)dV. \tag{A3}$$

Defining a body force distribution $f^c_i \equiv -\partial_j\sigma^c_{ij}$, i.e. $f^c_i = -c_{ijkl}\partial_j\Delta^c_{kl} = \partial_j\sigma^o_{ij}$, and employing the identities $\partial_j\left(\sigma^o_{ij}u^c_i\right) = \partial_j\sigma^o_{ij}u^c_i + \sigma^o_{ij}\partial_j u^c_i$, and $\int_{\partial\Omega}\sigma^o_{ij}u_i n_j dS = 0$, the relaxation energy is:

$$\Delta F = \int_\Omega \left(-f^c_i u^c_i + \frac{1}{2}c_{ijkl}\Delta^c_{ij}\Delta^c_{kl}\right)dV. \tag{A4}$$

For a repeating supercell structure or a dilute Fe–C concentration considered here:

$$f^c_i(\mathbf{r}) = \frac{1}{\Omega}\sum_{\mathbf{K}}\tilde{f}_i(\mathbf{K})e^{i\mathbf{K}\cdot\mathbf{r}}, \tag{A5}$$

where $\tilde{f}_i(\mathbf{K}) = \int_\Omega f^c_i(\mathbf{r})e^{-i\mathbf{K}\cdot\mathbf{r}}dV$, and $\mathbf{K}$ is a reciprocal lattice vector. For a large volume Ω, the magnitude of $\mathbf{K}$ is considered to be small. Hence $\tilde{f}_i(\mathbf{K})$ can be expanded to the first nonvanishing term in a Taylor series expansion in $\mathbf{K}$ as:

$$\tilde{f}_i(\mathbf{K}) = \int_\Omega f^c_i(\mathbf{r})(1 - iK_j r_j + \cdots)dV. \tag{A6}$$

Since the crystal has inversion symmetry around the origin taken to coincide with the solute atom position, the body force $f^c_i(\mathbf{r})$ acquires the symmetry $f^c_i(-\mathbf{r}) = -f^c_i(\mathbf{r})$, which enables us to write:

$$\begin{aligned}\tilde{f}_i(\mathbf{K}) &= -iK_j\int_\Omega f^c_i(\mathbf{r})r_j dV + O(K^3)\\ &= -iK_j\Omega\bar{\Gamma}_{ij} + O(K^3),\end{aligned} \tag{A7}$$

where $\Omega\bar{\Gamma}_{ij} \equiv \int_\Omega f^c_i r_j dV$. The term $\Omega\bar{\Gamma}_{ij}$ has appeared in the literature [15,16] as the elastic dipole moment of a point source. It can be easily shown that the body force $f^*_i(\mathbf{r}) = -\Gamma^o_{ij}\partial_j\delta(\mathbf{r})$ yields same Fourier components as in Eq. (A7), except only for the higher-order terms [12]. By replacing $f^c_i(\mathbf{r})$ with $f^*_i(\mathbf{r})$, the relaxation energy is:

$$\Delta F = \int_\Omega \left(-\Gamma^o_{ij}\delta(\mathbf{r})\Delta^c_{ij} + \frac{1}{2}c_{ijkl}\Delta^c_{ij}\Delta^c_{kl}\right)dV, \tag{A8}$$

where the identity $\int_\Omega \partial_i(\delta(\mathbf{r})u^c_i)dV = \int_\Omega \partial_j\delta(\mathbf{r})u^c_i dV + \int_\Omega \delta(\mathbf{r})\partial_j u^c_i dV = 0$ is used. The relaxation energy then resembles relaxation of a concentrated stress source:

$$\sigma^o_{ij} = -\Gamma^o_{ij}\delta(\mathbf{r}), \tag{A9}$$

located at the origin, as noted by Daw [36].

The distortional field can be written in terms of the Fourier summation:

$$\Delta^c_{ij}(\mathbf{r}) = \frac{1}{\Omega}\sum_{\mathbf{K}}\widetilde{\Delta}^c_{ij}(\mathbf{K})e^{i\mathbf{K}\cdot\mathbf{r}}, \tag{A10}$$

where $\widetilde{\Delta}^c_{ij}(\mathbf{K}) = \int_\Omega \Delta^c_{ij}(\mathbf{r})e^{-i\mathbf{K}\cdot\mathbf{r}}dV$. In terms of the variable $\mathbf{K}$, the relaxed energy is:

$$\Delta F = \frac{1}{2\Omega}\sum_{\mathbf{K}}c_{ijkl}\widetilde{\Delta}^c_{ij}(\mathbf{K})\widetilde{\Delta}^{c*}_{kl}(\mathbf{K}) - \frac{1}{\Omega}\sum_{\mathbf{K}}\Gamma^o_{ij}\widetilde{\Delta}^{c*}_{ij}(\mathbf{K}). \tag{A11}$$

The considered supercell does not contain any dislocations, and hence is curl free. Daw [36] has shown that the solution of the distortional field for $\mathbf{K} \neq 0$ term has the form:

$$\widetilde{\Delta}^c_{ij} = K_i[\mathbf{A}^{-1}]_{jl}\Gamma^o_{kl}K_k, \tag{A12}$$

where $A_{jl} = c_{ijkl}K_iK_k$.

For the $\mathbf{K} = 0$ term or $\widetilde{\Delta}^o_{ij}$, the solution can be determined by minimizing the relaxed energy with respect to $\widetilde{\Delta}^o_{ij}$, yielding:

$$c_{ijkl}\widetilde{\Delta}^o_{kl} = \Gamma^o_{ij}, \quad \text{or} \quad \widetilde{\Delta}^o_{ij} = s_{ijkl}\Gamma^o_{kl}. \tag{A13}$$

Eq. (A13) shows that the strength of the elastic field of a point source of dilation is related to the shape and volume changes of the relaxed periodic structures. Therefore, the strength of elastic dipole Γ^o_{ij} can be determined from homogeneous relaxation of the supercell with respect to both the internal coordinates and the supercell dimensions.

Consider the first variant of the solute field where a solute is inserted into an x_1-type octahedral interstitial site $\left(\Gamma^o_{ij} = \Gamma^{o(1)}_{ij}\right)$. The changes in supercell lattice parameters L_1, L_2, and L_3 are:

$$\Delta L_1 = \int_0^{L_o}\Delta^c_{11}(x_1,0,0)dx_1, \quad \Delta L_2 = \int_0^{L_o}\Delta^c_{22}(0,x_2,0)dx_2, \tag{A14}$$

with $\Delta L_2 = \Delta L_3$ by symmetry. In terms of the Fourier-transform variable $\mathbf{K}$, Eq. (A14) becomes:

$$\Delta L_1 = \frac{L_o}{\Omega}\sum_{K_2,K_3}\widetilde{\Delta}^c_{11}(0,K_2,K_3), \quad \Delta L_2 = \frac{L_o}{\Omega}\sum_{K_1,K_3}\widetilde{\Delta}^c_{22}(K_1,0,K_3). \tag{A15}$$

It can be shown that the terms $\widetilde{\Delta}^c_{11}(0,K_2,K_3)$ and $\widetilde{\Delta}^c_{22}(K_1,0,K_3)$ vanish for every $\mathbf{K} \neq 0$. The strength of the dipole moment thus relates to the relaxed strains ε^T_1 and ε^T_2 by:

$$\varepsilon^T_1 = \frac{\Delta L_1}{L_o} = \frac{1}{\Omega}s_{11ij}\Gamma^{o(1)}_{ij}, \quad \text{and} \quad \varepsilon^T_2 = \frac{\Delta L_2}{L_o} = \frac{1}{\Omega}s_{22ij}\Gamma^{o(1)}_{ij}. \tag{A16}$$

Eq. (A16) can be inverted to determine components of $\Gamma^{o(1)}_{ij}$. Performing the inversion, one finds:

$$\begin{aligned}\Gamma^o_{11} &= \Omega\left[C_{11}\varepsilon^T_1 + 2C_{12}\varepsilon^T_2\right], \quad \text{and}\\ \Gamma^o_{22} &= \Omega\left[C_{11}\varepsilon^T_1 + C_{12}(\varepsilon^T_1 + \varepsilon^T_2)\right].\end{aligned} \tag{A17}$$

If Vegard's law holds, the change of the supercell lattice parameters are linear in the interstitial mole fraction of the solute n or:

$$\begin{aligned}L_1(n) &= L_o + n\frac{dL_1}{dn}|_{n=0}\\ L_2(n) &= L_o + n\frac{dL_2}{dn}|_{n=0}.\end{aligned} \tag{A18}$$

The relaxed strains are thus:

$$\varepsilon^T_1 = n\eta^c, \quad \text{and} \quad \varepsilon^T_2 = n\eta^a, \tag{A19}$$

where η^c and η^a are the relative changes in the supercell lattice parameters with respect to an insertion of a C solute atom, given by:

$$\eta^c = \frac{1}{L_o}\frac{dL_1}{dn}|_{n=0}, \quad \text{and} \quad \eta^a = \frac{1}{L_o}\frac{dL_2}{dn}|_{n=0}. \tag{A20}$$

Also, in bcc crystals the number of the host atoms is equal to the number of the primitive cells. An insertion of a single solute into one of the octahedral interstices leads to:

$$n\Omega = v_o, \tag{A21}$$

where v_o is the primitive cell volume. We now substitute Eqs. (A19) and (A21) into Eq. (A17) to find:

$$\begin{aligned} \Gamma^o_{11} &= v_o(C_{11}\eta^c + 2C_{12}\eta^a), \quad \text{and} \\ \Gamma^o_{22} &= v_o(C_{11}\eta^c + C_{12}(\eta^c + \eta^a)). \end{aligned} \tag{A22}$$

Eq. (A22) can be written more compactly by collecting η^c and η^a into a relative transformation tensor:

$$\boldsymbol{\eta}^{(1)} = \begin{pmatrix} \eta^c & 0 & 0 \\ 0 & \eta^a & 0 \\ 0 & 0 & \eta^a \end{pmatrix}, \tag{A23}$$

which, for a cubic material, enables us to write:

$$\Gamma^{o(1)}_{ij} = \Omega c_{ijkl}\eta^{(1)}_{kl} n = v_o c_{ijkl}\eta^{(1)}_{kl}. \tag{A24}$$

Finally, substitution of Eq. (A24) into Eq. (1) leads to:

$$F^{int(1)} = -v_o c_{ijkl}\eta^{(1)}_{kl}\Delta^d_{ij}, \tag{A25}$$

which relates the interaction energy directly to the lattice contraction and the expansion of the relaxed structure.

The relative transformation tensors of the other two variants are:

$$\boldsymbol{\eta}^{(2)} = \begin{pmatrix} \eta^a & 0 & 0 \\ 0 & \eta^c & 0 \\ 0 & 0 & \eta^a \end{pmatrix}, \quad \text{and} \quad \boldsymbol{\eta}^{(3)} = \begin{pmatrix} \eta^a & 0 & 0 \\ 0 & \eta^a & 0 \\ 0 & 0 & \eta^c \end{pmatrix}. \tag{A26}$$

The interaction of the dislocation with these variants of the solute field is obtained by appropriately replacing $\eta^{(1)}_{kl}$ with $\eta^{(2)}_{kl}$ or $\eta^{(3)}_{kl}$ in Eq. (A25).

References

[1] Cottrell AH, Jaswon MA. Proc Roy Soc A 1949;199:104.
[2] Hirth JP, Lothe H. Theory of dislocations. New York: John Wiley; 1971.
[3] Miller MK. Microsc Res Tech 2006;69:359.
[4] Cochardt AW, Schoeck G, Wiedersich H. Acta Metall 1955;3:533.
[5] Bacon DJ. Scripta Metall 1969;3:735.
[6] Douthwaite RM, Evans J. Scripta Metall 1973;7:1019.
[7] Clouet E, Garruchet S, Nguyen H, Perez M, Becquart CS. Acta Mater 2008;56:3450.
[8] Bernshtein ML, Kaputkina LM, Prokoshkin SD. Phys Met Metallogr 1981;52:127.
[9] Cadeville MC, Friedt JM, Lerner C. J Phys F 1977;7:123.
[10] Ohman E. JISI 1931;130:445.
[11] Cheng L, Bottger A, de Keijser TH, Mittemeijer E. Scripta Metall 1990;25:509.
[12] Eshelby JD. Solid State Phys 1956;3:79.
[13] Eshelby JD. Prog Solid Mech 1961;2:89.
[14] Kohn W, Sham LJ. Phys Rev 1965;140:A1113.
[15] DeFontaine D. Solid State Phys 1979;34:79.
[16] Kroner K. Physics of defects. New York: North-Holland; 1981.
[17] Khachaturyan AG. Theory of structural transformations in solids. New York: John Wiley; 1983.
[18] Khachaturyan AG, Semenovskaya S, Tsakalakos T. Phys Rev B 1995;52:15909.
[19] Li DY, Chen LQ. Acta Mater 1997;45:2435.
[20] Li DY, Chen LQ. Acta Mater 1998;46:639.
[21] The elastic constants of Fe are certainly impacted by the fact that Fe is ferromagnetic. Hence the Γ^o_{ij}'s appearing in Eq. (1) already reflect, to a certain extent, the importance of magnetism. The implementation in Eq. (5), however, allows the magnetic and electronic structure to change with local changing strains, and thereby enables further assessment.
[22] Kresse G, Furthmuller J. Phys Rev B 1996;54:11169.
[23] Clatterbuck DM, Chrzan DC, Morris JW. Acta Mater 2003;51:2271.
[24] Rayne JA, Chandrasekhar BS. Phys Rev 1961;122:1714.
[25] Stroh AN. J Math Phys 1962;41:77.
[26] Daw MS, Baskes MI. Phys Rev Lett 1983;50:1285.
[27] Daw MS, Baskes MI. Phys Rev B 1984;29:6443.
[28] Cheng R. Fundamental aspects of dislocation theory, vol. 317. Gaithersburg (MD): NBS Special Publication; 1970. p. 299.
[29] Hosson JTMD. Solid State Commun 1975;15:747.
[30] Shu X, Wang C. Mater Sci Forum 2007;1865:561.
[31] Tapasa K, Osetsky YN, Bacon DJ. Acta Mater 2007;93:55.
[32] Becquart C, Raulot J, Bencteux G, Domain C, Perez M, Garruchet S, et al. Comput Mater Sci 2007;40:119.
[33] Louat N. Proc Phys Soc Lond 1956;B68:459.
[34] Beshers DN. Acta Metall 1958;6:521.
[35] Mura T. Adv Mater Res 1968;3:1.
[36] Daw MS. Comput Mater Sci 2006;38:293.